2024 IEEE/RSJ International Conference on Intelligent Robots and Systems (IROS)
October 14-18, 2024. Abu Dhabi, UAE

Voltage Regulation in Polymer Electrolyte Fuel Cell Systems Using Gaussian Process Model Predictive Control

Xiufei Li[1†], Miao Yang[3†], Miao Zhang[2*], Yuanxin Qi[1], Zhuowei Li[4], Senbin Yu[5], Yuantao Wang[6], Linpeng Shen[2], Xiang Li[7]

***Abstract*— This study presents a novel approach using Gaussian process model predictive control (MPC) to stabilize the output voltage of a polymer electrolyte fuel cell (PEFC) by regulating hydrogen and airflow rates. Two Gaussian process models capture PEFC dynamics, accounting for constraints like hydrogen pressure and input change rates to reduce predictive control errors. The performance of the physical model and Gaussian process MPC in handling constraints and system inputs is compared. Simulations show that the proposed Gaussian process MPC maintains the voltage at 48 V while adhering to safety constraints, even with workload disturbances from 110-120 A. Compared to traditional MPC with detailed system models, Gaussian process MPC has similar overshoot and slower response time but requires less system information and no underlying true system model.**

I. INTRODUCTION

Due to the adverse environmental consequences associated with traditional fossil fuels and their contribution to global warming, PEFCs have emerged as highly promising power sources owing to their utilization of renewable energy sources, high energy efficiency, and low operating temperatures [1], [2]. While PEFCs are increasingly favored across stationary, portable, and transportation applications, their commercialization remains hampered by various technical challenges, with ensuring reliable operation standing out as a major hurdle [3]. Control algorithms play a pivotal role in enhancing the reliability of PEFC systems. However, the complexity of PEFC systems, characterized by numerous input parameters and safety constraints, necessitates the adoption of more sophisticated control methodologies [4].

MPC controllers distinguish themselves in PEFC systems' control applications due to their robust handling of multiple inputs and constraints, making them widely utilized across various PEFC system applications. Quan et al. [5] introduced a multi-input multi-output (MIMO) MPC to regulate hydrogen excess ratio and balance electrode pressures. Hahn et al. [6] proposed an MPC-based operation strategy for controlling an automotive fuel cell air system. Their study demonstrated that the MPC approach could potentially reduce hydrogen consumption by 3% while decreasing the risk of harmful operating conditions compared to a validated map-based operation strategy. Long et al. [7] devised a master-slave MPC method for current-sharing control in systems, demonstrating the feasibility and effectiveness of the proposed MPC-based current-sharing strategy. Recent studies have showcased various approaches to MPC applications, highlighting its efficacy and promise as a control method. The MPC models employed in the aforementioned research, however, primarily rely on physical models. The modeling process entails numerous partial differential equations, and simplifying them necessitates expert knowledge and is time-intensive. Conversely, data-based modeling leverages observed data rather than intrinsic physical laws to derive the system model. Data-based models have garnered increasing attention due to their robust representation capabilities, flexibility, and ease of construction. The MPC control approaches derived from these data-driven models hold appeal for fuel cell applications, given the nonlinearity and complexity inherent in fuel cell systems [8], [9]. While one frequently employed data-based method is the Gaussian process (GP) [10]. Unlike optimizing parameters of selected functions to fit data, GP searches for relationships between measured data. He et al. [11] employed a nonparametric Gaussian process regression model to capture the nonlinear relationship between operating conditions and output voltage in microbial fuel cells. They also proposed a simple online learning strategy for recursively updating model hyperparameters. Zhu et al. [12] applied Gaussian process state-space models to analyze fuel cell degradation and incorporated prediction confidence intervals to enhance inference accuracy. Zhang et al. [13] constructed a Gaussian process regression model to predict methane conversion rates in solid oxide fuel cells. However, a comprehensive model was lacking to consider the constraints associated with control variables and hydrogen pressure. This paper addresses this gap by imposing limits on both control variables and hydrogen pressure to ensure safe operation. Specifically, when utilized as a power generation source, a fuel-cell system must deliver a stable and consistent voltage [14]. In our previous study [15], a novel MPC approach was devised to regulate the output voltage of the PEFC system to a steady state by simultaneously adjusting its input hydrogen and air volumetric flow rates. The capability of the Gaussian process MPC to manage the fuel cell system under constraints is thoroughly investigated, and a performance comparison between MPC based on physical models and Gaussian process MPC is presented.

[1]Lund University, Department of Energy Sciences, Lund, 22100, Sweden
[2]Shenzhen International Graduate School, Tsinghua University, Shenzhen 518055, China
[3]Nanyang Technological University, College of Computing and Data Science, Singapore
[4]The University of Nottingham, China
[5]Gala Sports, China
[6]Beijing University of Technology, China
[7]Nantong University, China
*Corresponding author: Miao Zhang, zhangmiaotju@gmail.com
†First Author and Second Author contribute equally to this work.

II. Gaussian process modeling

A. Gaussian process

Gaussian process is a probabilistic, non-parametric black-box model that is defined as a collection of random variables. Any finite number of variables from this collection have a joint Gaussian distribution [16]. Gaussian process $\mathcal{GP}$ can be fully characterized by a mean function $\bar{f}(\boldsymbol{x})$ and covariance function $k(\boldsymbol{x}, \boldsymbol{x}')$,

$$f(\boldsymbol{x}) \sim \mathcal{GP}\left(\bar{f}(\boldsymbol{x}), k(\boldsymbol{x}, \boldsymbol{x}')\right), \tag{1}$$

where $\boldsymbol{x}$ and $\boldsymbol{x}'$ both are data point with dimension d. $k(\boldsymbol{x}, \boldsymbol{x}')$ is also called the kernel function. $\bar{f}(\boldsymbol{x})$ is assumed to be zero for simplicity.

The observations y are denoted by the variable

$$y = f(\boldsymbol{x}) + e, \quad e \sim \mathcal{N}(0, \sigma_n^2), \tag{2}$$

where e is the additive independent identically distributed Gaussian noise $\mathcal{N}$ with variance σ_n^2.

Assuming there are n training points and n^* test points when making inferences, the prior is

$$\begin{bmatrix} \boldsymbol{y} \\ \boldsymbol{f}^* \end{bmatrix} \sim \mathcal{N}\left(\boldsymbol{0}, \begin{bmatrix} K(\boldsymbol{X}, \boldsymbol{X}) + \sigma_n^2 \boldsymbol{I} & K(\boldsymbol{X}, \boldsymbol{X}^*) \\ K(\boldsymbol{X}^*, \boldsymbol{X}) & K(\boldsymbol{X}^*, \boldsymbol{X}^*) \end{bmatrix}\right), \tag{3}$$

where $(\boldsymbol{X}, \boldsymbol{y})$ are the training data with dimension $n \times d$ and $n \times 1$ respectively; $\boldsymbol{X}^*$ are the test data points with dimension $n^* \times d$ on which the prediction is made; $\boldsymbol{f}^*$ are the n^* dimension predicted value; $K(\boldsymbol{X}, \boldsymbol{X}^*)$ denotes the $n \times n^*$ matrix of the covariances evaluated at all pairs of training and test points, and similarly for $K(\boldsymbol{X}, \boldsymbol{X})$, $K(\boldsymbol{X}^*, \boldsymbol{X}^*)$ and $K(\boldsymbol{X}^*, \boldsymbol{X})$.

The posterior is

$$\boldsymbol{f}^* | \boldsymbol{X}^*, \boldsymbol{X}, \boldsymbol{y} \sim \mathcal{N}\left(\mathrm{E}\{\boldsymbol{f}^*\}, \mathrm{cov}\{\boldsymbol{f}^*\}\right), \tag{4}$$

where

$$\begin{aligned} \mathrm{E}\{\boldsymbol{f}^*\} = &\ K(\boldsymbol{X}^*, \boldsymbol{X})\left[K(\boldsymbol{X}, \boldsymbol{X}) + \sigma_n^2 \boldsymbol{I}\right]^{-1} \boldsymbol{y} \quad \text{and} \\ \mathrm{cov}\{\boldsymbol{f}^*\} = &\ K(\boldsymbol{X}^*, \boldsymbol{X}^*) - K(\boldsymbol{X}^*, \boldsymbol{X})\left[K(\boldsymbol{X}, \boldsymbol{X}) + \sigma_n^2 \boldsymbol{I}\right]^{-1} \\ & K(\boldsymbol{X}, \boldsymbol{X}^*). \end{aligned} \tag{5}$$

General GP regression is equivalent to Bayesian linear regression with an infinite number of basis functions. The kernel function adopted in this work is the squared exponential kernel (Gaussian kernel). The squared exponential kernel k_{SE} is defined as

$$k_{SE}(\boldsymbol{x}, \boldsymbol{x}') = \sigma^2 \exp\left(\frac{-\|\boldsymbol{x} - \boldsymbol{x}'\|^2}{2l^2}\right), \tag{6}$$

where l is the length scale and σ is the signal standard deviation. $\|\boldsymbol{x} - \boldsymbol{x}'\|$ is the Euclidean norm, representing the distance between $\boldsymbol{x}$ and $\boldsymbol{x}'$.

The length scale l can be interpreted as a measure of how closely the points $\boldsymbol{x}$ and $\boldsymbol{x}'$ need to be to significantly influence each other. When the length scale l is a scalar, the kernel is considered isotropic. In contrast, if l varies for each dimension of the data points, the kernel is referred to as an automatic relevance determination (ARD) kernel [16]. The ARD kernel allows the model to determine the relevance of each dimension separately, providing a feature selection ability. In this case, the expressions related to the length scale in Eq. (6) are modified to a summation form. Additionally, the model's flexibility can be extended by adding multiple kernels.

The optimal parameters of the GP are found by maximizing the log marginal likelihood p,

$$\log p(\boldsymbol{y} | \boldsymbol{X}, \boldsymbol{\theta}) = -\frac{1}{2}\boldsymbol{y}^T \boldsymbol{K}_y^{-1} \boldsymbol{y} - \frac{1}{2}\log \|\boldsymbol{K}_y\| - \frac{n}{2}\log 2\pi, \tag{7}$$

where $\boldsymbol{K}_y = K(\boldsymbol{X}, \boldsymbol{X}) + \sigma_n^2 \boldsymbol{I}$ is the covariance matrix for the noisy targets $\boldsymbol{y}$ and n is the number of training points. $\boldsymbol{\theta}$ are the hyperparameters, including the length scale of each dimension and signal and noise variance [16].

B. Gaussian process for fuel cell modeling

In our previous work [15], a detailed physical fuel cell system model was elaborated and built with MATLAB Simulink, which was assumed the closest to the true system dynamics. To model errors in measurement, Gaussian measurement noises were added to output voltage V_{FC} and hydrogen pressure $P_{\mathrm{H_2}}$.

The Gaussian process model predicts two system states based on three system inputs. These inputs include the control actions, i.e., hydrogen volumetric flow rate $Q_{\mathrm{H_2}}$, air volumetric flow rate Q_{air}, and the current I. The predicted states are the fuel cell output voltage V_{FC} and the hydrogen pressure $P_{\mathrm{H_2}}$. It is important to note that the current I represents the workload and cannot be manipulated by the controller. The control target is to maintain a fixed value for the fuel cell voltage, while the hydrogen pressure must be kept below a certain limit to ensure safety.

The target of GP modeling is to build a function $\boldsymbol{f}$ that describes the fuel cell dynamics in the time update $\boldsymbol{x}^{k+1}$,

$$\boldsymbol{x}^{k+1} = \boldsymbol{f}(\boldsymbol{u}^k, \boldsymbol{x}^k), \tag{8}$$

where

$$\boldsymbol{u}^k = [Q_{\mathrm{H_2}}^k \ Q_{\mathrm{air}}^k \ I^k]^T \quad \text{and} \quad \boldsymbol{x}^k = [V_{\mathrm{FC}}^k \ P_{\mathrm{H_2}}^k]^T, \tag{9}$$

in which the variable $\boldsymbol{x}^{k+1}$ is the system states at time step $k+1$. $\boldsymbol{u}^k$ and $\boldsymbol{x}^k$ are the model inputs and measured system states at time step k, respectively.

The Gaussian process, however, doesn't support multi-dimensional regression natively. One simple solution is to assume the multi-dimensional states are independent and build a Gaussian process for each state with the same inputs. Eq. (8) then becomes two Gaussian processes f_V and f_P,

$$V_{\mathrm{FC}}^{k+1} = f_V(\boldsymbol{u}^k, V_{\mathrm{FC}}^k) \quad \text{and} \quad P_{\mathrm{H_2}}^{k+1} = f_P(\boldsymbol{u}^k, P_{\mathrm{H_2}}^k). \tag{10}$$

To collect the training data points for the Gaussian process, Latin hypercube sampling (LHS) was applied to the inputs $Q_{\mathrm{H_2}}$, Q_{air} and the current I.

The kernel type used for the two Gaussian processes was a combination of an isotropic squared exponential kernel

(Gaussian kernel) and an automatic relevance determination (ARD) squared exponential kernel. The parameters of the Gaussian process model were selected by maximizing the log-likelihood function described in Eq. (7). Solving this optimization problem is typically challenging due to its nonlinearity and nonconvexity. In this study, the limited-memory Broyden–Fletcher–Goldfarb–Shanno (L-BFGS) algorithm [17] was employed to efficiently solve the problem.

After training, the GP model was validated using testing data points. These testing data points were obtained by applying a different set of Latin Hypercube Sampling (LHS) inputs to the fuel cell Simulink model. The prediction results are depicted in Fig. 1, where the blue line represents the true values and the orange line represents the one-step predictions made by the GP model. The orange shaded area represents the one σ confidence interval, which is the prediction value plus/minus one prediction standard deviation (one σ).

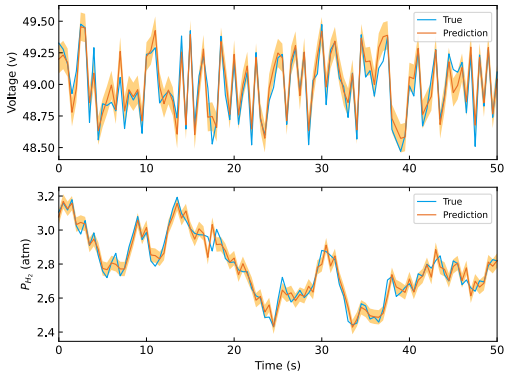

Fig. 1. Gaussian process training results. The orange shaded area is the one σ confidence interval, the prediction value plus/minus one prediction standard deviation (one σ).

It is evident from the results that the GP model accurately predicted the behavior of the fuel cell in terms of V_{FC} and $P_{\mathrm{H_2}}$. The variance calculated by the GP model served as an indicator of the prediction confidence. The width of the prediction band was wider in regions where the test points were far from the training points, indicating lower prediction accuracy by the GP model. However, in the majority of cases, the prediction band was able to encompass the true value.

III. Gaussian Process MPC Design

The state-space model for MPC is derived by linearizing the Gaussian process models. Consequently, the Gaussian process f_V in Eq. (10) becomes

$$\mathrm{d}V_{\mathrm{FC}} = \begin{bmatrix} \dfrac{\partial f_V}{\partial Q_{\mathrm{H_2}}} & \dfrac{\partial f_V}{\partial Q_{\mathrm{air}}} & \dfrac{\partial f_V}{\partial I} \end{bmatrix} \begin{bmatrix} \mathrm{d}Q_{\mathrm{H_2}} \\ \mathrm{d}Q_{\mathrm{air}} \\ \mathrm{d}I \end{bmatrix}, \tag{11}$$

where the partial derivative is taken on the latest system states, which will update each time step. The partial derivative of the GP with Gaussian kernel can be solved explicitly, but the forward mode automatic differentiation (AD) method [18] is used here for simplicity and flexibility. The same expression is true for the Gaussian process f_P.

The discrete-time state-space model of the fuel cell used for control is written as

$$\boldsymbol{x}^{k+1} = \boldsymbol{A}\boldsymbol{x}^k + \boldsymbol{B}\boldsymbol{u}^k \qquad \text{and} \qquad \boldsymbol{y}^k = \boldsymbol{C}\boldsymbol{x}^k, \tag{12}$$

where the state vector $\boldsymbol{x}^k$ at sample index k is

$$\boldsymbol{x}^k = \begin{bmatrix} V_{\mathrm{FC}}^k \\ P_{\mathrm{H_2}}^k \\ \mathrm{d}I^k \\ Q_{\mathrm{H_2}}^k \\ Q_{\mathrm{air}}^k \end{bmatrix} \qquad \text{with input} \qquad \boldsymbol{u}^k = \begin{bmatrix} \mathrm{d}Q_{\mathrm{H_2}}^k \\ \mathrm{d}Q_{\mathrm{air}}^k \end{bmatrix}$$
$$\text{and output} \qquad \boldsymbol{y}^k = \begin{bmatrix} V_{\mathrm{FC}}^k \end{bmatrix}, \tag{13}$$

and state-space matrices

$$\begin{aligned} \boldsymbol{A} &= \begin{bmatrix} 1 & 0 & \frac{\partial f_V}{\partial I} & 0 & 0 \\ 0 & 1 & \frac{\partial f_P}{\partial I} & 0 & 0 \\ 0 & 0 & 0 & 0 & 0 \\ 0 & 0 & 0 & 1 & 0 \\ 0 & 0 & 0 & 0 & 1 \end{bmatrix}, \\ \boldsymbol{B} &= \begin{bmatrix} \frac{\partial f_V}{\partial Q_{\mathrm{H_2}}} & \frac{\partial f_V}{\partial Q_{\mathrm{air}}} \\ \frac{\partial f_P}{\partial Q_{\mathrm{H_2}}} & \frac{\partial f_P}{\partial Q_{\mathrm{air}}} \\ 0 & 0 \\ 1 & 0 \\ 0 & 1 \end{bmatrix}, \\ \boldsymbol{C} &= \begin{bmatrix} 1 & 0 & 0 & 0 & 0 \end{bmatrix}. \end{aligned} \tag{14}$$

The actuator increments were selected as the system inputs. Consequently, $Q_{\mathrm{H_2}}^k$ and Q_{air}^k were added into the state vector to help impose appropriate constraints.

A Quadratic Programming (QP) problem will be solved at each time step to obtain the optimal control inputs in this MPC problem formulation

$$\begin{aligned} \min_{\boldsymbol{u}^0, \boldsymbol{u}^1, \ldots, \boldsymbol{u}^{H_u}{}_1} \boldsymbol{J}(\boldsymbol{u}^k) = &\sum_{k=1}^{H_p} \left\| \boldsymbol{y}^k - \boldsymbol{r} \right\|_{\boldsymbol{Q}}^2 + \sum_{k=0}^{H_u - 1} \left\| \boldsymbol{u}^k \right\|_{\boldsymbol{R}}^2 \\ &+ \rho \sum_{k=1}^{H_p} \left\| \boldsymbol{\epsilon}^k \right\|^2, \end{aligned} \tag{15}$$

subject to:

$$\begin{aligned} \boldsymbol{x}^{k+1} &= \boldsymbol{A}^{\boldsymbol{d}}\boldsymbol{x}^k + \boldsymbol{B}^{\boldsymbol{d}}\boldsymbol{u}^k, \\ \boldsymbol{y}^k &= \boldsymbol{C}^{\boldsymbol{d}}\boldsymbol{x}^k, \\ \boldsymbol{u}_{\mathrm{lb}} &\le \boldsymbol{u}^k \le \boldsymbol{u}_{\mathrm{ub}}, \\ \mathrm{d}\boldsymbol{u}_{\mathrm{lb}} &\le \boldsymbol{u}^k - \boldsymbol{u}^{k-1} \le \mathrm{d}\boldsymbol{u}_{\mathrm{ub}}, \\ \boldsymbol{x}_{\mathrm{lb}} &\le \boldsymbol{x}^k \le \boldsymbol{x}_{\mathrm{ub}} + \boldsymbol{\epsilon}^k, \\ \boldsymbol{0} &\le \boldsymbol{\epsilon}^k, \\ P_{\mathrm{H_2}}^k &\le P_{\mathrm{H_2}}^{limit} + \epsilon^k, \\ P_{\mathrm{H_2}}^k &\le P_{\mathrm{H_2}}^{limit} + \epsilon^k - \alpha\sigma_p\Delta P_{\mathrm{H_2}}, \\ \boldsymbol{u}^{-1} &= \boldsymbol{u}_{\mathrm{init}}, \\ \boldsymbol{x}^0 &= \boldsymbol{x}_{\mathrm{init}}, \qquad \text{and} \\ k &= 0, 1, \ldots, H_p, \end{aligned} \tag{16}$$

where H_p and H_u are prediction and control horizon; k in the superscript represents the time step, and $k = 0$ refers

to the current time step; $\boldsymbol{r}$ is the control reference; $\boldsymbol{Q}$ and $\boldsymbol{R}$ are weight tuning parameters for reference tracking and control inputs; $\boldsymbol{A^d}$, $\boldsymbol{B^d}$, and $\boldsymbol{C^d}$ are state-space matrices $\boldsymbol{A}$, $\boldsymbol{B}$ and $\boldsymbol{C}$ in discrete-time; $\boldsymbol{u}_{\mathrm{lb}}$, $\boldsymbol{u}_{\mathrm{ub}}$, $\boldsymbol{x}_{\mathrm{lb}}$, and $\boldsymbol{x}_{\mathrm{ub}}$ are the lower bounds and upper bounds of inputs $\boldsymbol{u}$ and states $\boldsymbol{x}$; $\mathrm{d}\boldsymbol{u}_{\mathrm{lb}}$ and $\mathrm{d}\boldsymbol{u}_{\mathrm{ub}}$ are the lower bounds and upper bounds of inputs change rate; $\boldsymbol{u}_{\mathrm{init}}$ is latest applied control inputs and $\boldsymbol{x}_{\mathrm{init}}$ is the latest measured value, the state feedback; $P_{\mathrm{H_2}}^{limit}$ is the upper bound of $P_{\mathrm{H_2}}$; $\boldsymbol{\epsilon}$ is the slack variable introduced to soft constraints and ρ is a non-negative scalar to control the magnitude of penalizing soft constraint violations.

The additional inequality for $P_{\mathrm{H_2}}$ as a compensation for model errors is

$$P_{\mathrm{H_2}}^k \leq P_{\mathrm{H_2}}^{limit} + \epsilon^k - \alpha\sigma_p \Delta P_{\mathrm{H_2}}, \tag{17}$$

where σ_p is the prediction variance when making inference with Gaussian process f_P on the data point in the current time step; $\Delta P_{\mathrm{H_2}}$ is the possible $P_{\mathrm{H_2}}$ move with respect to the possible calculated inputs

$$\Delta P_{\mathrm{H_2}} = \sum_{i=0}^{k-1} (\mathrm{d}Q_{\mathrm{H_2}}^i \frac{\partial f_P}{\partial Q_{\mathrm{H_2}}} + \mathrm{d}Q_{\mathrm{air}}^i \frac{\partial f_P}{\partial Q_{\mathrm{air}}}), \tag{18}$$

α is a tuning parameter. This $\alpha\sigma_p\Delta P_{\mathrm{H_2}}$ term can be understood from an intuitive point of view. Typically, a bigger possible move will lead to a bigger uncertainty. Thus, a redundancy proportional to the possible movement size and prediction uncertainty in the constraint is desirable to compensate for the model imperfections. Since the $P_{\mathrm{H_2}}$ limit is from above, the added constraint in Eq. (17) is only meaningful when the possible move is positive.

To be precise, this constraint on $P_{\mathrm{H_2}}^k$ is simplified from the stochastic MPC constraint formation. In stochastic MPC, a chance constraint is

$$p(\boldsymbol{x}^k \leq \boldsymbol{x}_{\mathrm{ub}}) \geq \eta, \tag{19}$$

where η denotes the confidence level. When η is 0.95, it is

$$\boldsymbol{x}^k \leq \boldsymbol{x}_{\mathrm{ub}} - 2\Sigma^k, \tag{20}$$

where Σ^k is the covariance matrix of $\boldsymbol{x}^k$. Here $\boldsymbol{x}^k$ actually represents its mean value. The Σ^k is estimated from the uncertainty propagation. The specific form for $P_{\mathrm{H_2}}$ of Eq. (20) is:

$$P_{\mathrm{H_2}}^k \leq P_{\mathrm{H_2}}^{limit} - 2\sigma_p^k, \tag{21}$$

For every step in the prediction horizon, the $P_{\mathrm{H_2}}^k$ variance is propagated along with the uncertainty in $\boldsymbol{B}$ matrix. The linearized form

$$P_{\mathrm{H_2}}^{k+1} = P_{\mathrm{H_2}}^k + \mathrm{d}Q_{\mathrm{H_2}}^k \frac{\partial f_P}{\partial Q_{\mathrm{H_2}}} + \mathrm{d}Q_{\mathrm{air}}^k \frac{\partial f_P}{\partial Q_{\mathrm{air}}}, \tag{22}$$

The variance estimate update is

$$(\sigma_p^{k+1})^2 = (\sigma_p^k)^2 + (\mathrm{d}Q_{\mathrm{H_2}}^k)^2 \mathrm{var}(\frac{\partial f_P}{\partial Q_{\mathrm{H_2}}}) + (\mathrm{d}Q_{\mathrm{air}}^k)^2 \mathrm{var}(\frac{\partial f_P}{\partial Q_{\mathrm{air}}}), \tag{23}$$

The variance of the partial derivative taken at the initial step is approximated by

$$\begin{aligned} \mathrm{var}(\frac{\partial f_P}{\partial Q_{\mathrm{H_2}}}) &= \mathrm{var}(\frac{f_P(Q_{\mathrm{H_2}} + \delta Q_{\mathrm{H_2}}) - f_P(Q_{\mathrm{H_2}})}{\delta Q_{\mathrm{H_2}}}) \\ &= \frac{2}{(\delta Q_{\mathrm{H_2}})^2}(\sigma_p)^2 \\ &= \alpha_1 \mathrm{E}^2\{\frac{\partial f_P}{\partial Q_{\mathrm{H_2}}}\}(\sigma_p)^2, \end{aligned} \tag{24}$$

where $2/(\delta Q_{\mathrm{H_2}})^2$ is assumed to be proportional to $\mathrm{E}^2\{\partial f_P/\partial Q_{\mathrm{H_2}}\}$ value with a constant value α_1. The $\mathrm{E}\{\partial f_P/\partial Q_{\mathrm{H_2}}\}$ is actually the $\partial f_P/\partial Q_{\mathrm{H_2}}$ value calculated at the initial time step. Thus, at each time step in the prediction horizon, the variance increases with a magnitude of

$$\alpha_1(\sigma_p)^2(\mathrm{d}Q_{\mathrm{H_2}}^k)^2\mathrm{E}^2\{\frac{\partial f_P}{\partial Q_{\mathrm{H_2}}}\} + \alpha_2(\sigma_p)^2(\mathrm{d}Q_{\mathrm{air}}^k)^2\mathrm{E}^2\{\frac{\partial f_P}{\partial Q_{\mathrm{air}}}\}, \tag{25}$$

Summing over the steps until time step k, and viewing all constant-coefficient as the same, gives the total standard error of time step k

$$\sigma_p^k = \alpha\sigma_p \sum_{i=0}^{k-1} \sqrt{(\mathrm{d}Q_{\mathrm{H_2}}^k)^2\mathrm{E}^2\{\frac{\partial f_P}{\partial Q_{\mathrm{H_2}}}\} + (\mathrm{d}Q_{\mathrm{air}}^k)^2\mathrm{E}^2\{\frac{\partial f_P}{\partial Q_{\mathrm{air}}}\}}, \tag{26}$$

All constants are written together as α. However this form is too conservative for constraint handling and requires high computational effort. The root part is approximated as

$$\mathrm{d}Q_{\mathrm{H_2}}^k\mathrm{E}\{\frac{\partial f_P}{\partial Q_{\mathrm{H_2}}}\} + \mathrm{d}Q_{\mathrm{air}}^k\mathrm{E}\{\frac{\partial f_P}{\partial Q_{\mathrm{air}}}\}, \tag{27}$$

Then the Eq. (26) becomes

$$\sigma_p^k = \alpha\sigma_p\Delta P_{\mathrm{H_2}}, \tag{28}$$

where $\Delta P_{\mathrm{H_2}}$ is shown in the Eq.(18). This also gives an intuitive interpretation of the constraint redundancy. Meanwhile, the constant 2 and α are integrated into the coefficient α in the constraints described by Eq. (16). This does not necessarily give a 95% confidence level, and α should be tuned according to the performance and safety requirements.

In the fuel cell problem, the state constraint is the limitation of the hydrogen pressure $P_{\mathrm{H_2}}$. The hydrogen pressure in the pipe should be under a certain value to ensure safety, which is 2.5 atm here. Only slack variables for state upper bounds are introduced. The input $Q_{\mathrm{H_2}}$ is limited between 100 and 400 lpm (liters per minute) and Q_{air} is limited within 300 to 700 lpm. The change rate of the inputs is constrained within -40 to 20 lpm. The fuel cell system size is 6 kW.

The time step for the MPC controller is 0.5 s. The QP problem is solved at each step, then the solved $Q_{\mathrm{H_2}}$ + $\mathrm{d}Q_{\mathrm{H_2}}$ and Q_{air} + $\mathrm{d}Q_{\mathrm{air}}$ are applied to the fuel cell plant.

IV. Simulation set-up

The simulation of the controller performance was conducted on the Simulink model detailed in [15]. This model is viewed as the true system dynamics. Gaussian measurement noises were added to voltage V_{FC} and hydrogen pressure $P_{\mathrm{H_2}}$.

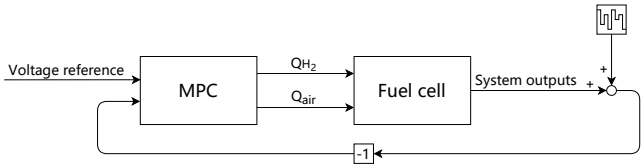

Fig. 2. MPC control process

Figure 2 gives the illustration of the MPC control process.

The formulation of MPC is shown in [15]. Besides, the constraints regarding the input change rate and hydrogen pressure were added.

The illustration of the GP MPC control process is shown in Fig. 3.

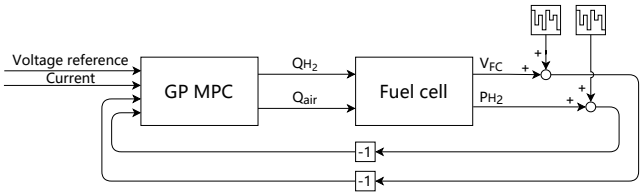

Fig. 3. GP MPC control process

Compared with the MPC controller shown in Fig. 2, the GP MPC only needs the system information of V_{FC} and $P_{\mathrm{H_2}}$, whereas MPC requires other information such as oxygen and nitrogen pressure. This is a desirable aspect in practice.

V. Simulation Results

The performance of GP-MPC and MPC with physical models explained in [15] were compared. Two test scenarios were chosen, one was the typical step disturbance applied on the working load, the current, and the other was a mixture of slope and step working load changes.

Figure 4 shows the GP MPC voltage tracking performance compared with MPC under step workload disturbance, and Fig. 5 presents the corresponding $P_{\mathrm{H_2}}$ behavior and system inputs. At the beginning of the experiment, MPC and GP MPC had similar rise-up traces, which were limited by the input change rate constraint. MPC had a lower overshoot than GP MPC benefiting from the accurate system model. The overshoot for GP MPC was 0.60 V and for MPC was 0.42 V. Both controllers can successfully satisfy the $P_{\mathrm{H_2}}$ safety requirements. When the current increased suddenly, MPC and GP MPC drove the voltage back to the reference at a similar pace, but MPC responded faster. To arrive at 47.9 V again, MPC took 5.2 s and GP MPC took 6.5 s. It can be seen that the inputs increased following a straight line, indicating the activation of the change rate limits. However, similar to the start of the system, the GP MPC calculated $Q_{\mathrm{H_2}}$ increment was rather conservative in comparison with MPC. This is because the added constraint in Eq. (17) enforced the controller to take a more cautious action when increasing $Q_{\mathrm{H_2}}$ which directly increased the $P_{\mathrm{H_2}}$. In contrast, Q_{air} was adjusted aggressively. When the current suddenly dropped at time 75 s, MPC and GP MPC had a similar performance in pulling back the voltage. The steady-state tracking behavior of the two controllers was comparable and the safety constraint was satisfied throughout the process.

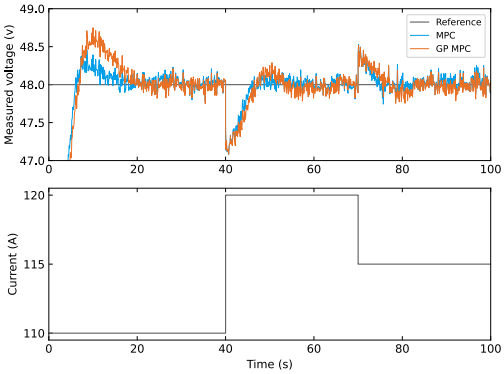

Fig. 4. Output voltage under the current step disturbance.

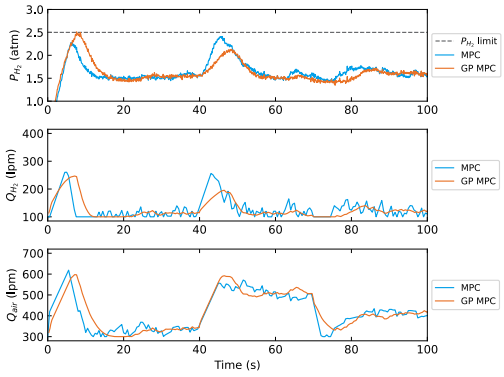

Fig. 5. Constraint handling and system inputs of MPC and GP MPC.

VI. Discussion

In the present work, a novel GP-MPC was the first known application of GP-MPC for fuel cell control. Although the MPC based on the physical model exhibited a slightly better performance in terms of the overshoot during system start-up, the GP MPC required less system information compared to the approach in [15], necessitating fewer sensors and being more economical. Despite being based on nonlinear GP models, the MPC framework utilized linearized models, thereby reducing the computational burden. In contrast, the nonlinear MPC described in [19] was more challenging to implement and solve. To compensate for model imperfections, a constraint accounting for prediction variance and possible moves was added, resulting in satisfactory constraint handling under model and linearization errors. Moreover, GP-MPC is a data-based model, unlike physics-based modeling, which does not rely on physical mechanisms. For very complex processes, physical modeling becomes more complicated, whereas data-based modeling is easier to implement in engineering applications. GP-MPC modeling not only provides predictions but also offers the confidence level of those predictions. Under

constrained conditions, the input behavior can be adjusted based on different confidence levels of the predictions, while ensuring both the performance of the controller and the satisfaction of constraints.

VII. Conclusion

A Gaussian process MPC was developed to control the fuel cell voltage. Two Gaussian processes were used to predict the voltage and hydrogen pressure. The state-space models were formed based on the linearized Gaussian process. A special inequality utilizing GP prediction variance was added to compensate for the model imperfections in satisfying constraints. The simulation results showed the GP MPC kept the voltage at the desired 48 V while satisfying the safety constraints including the hydrogen pressure limit of 2.5 atm and input change rate limit all the time under a workload disturbance ranging from 110-120 A. The constraint handling of GP MPC gave a conservative action, but the safety requirements were satisfied well benefiting from this characteristic. As compared to the MPC with the knowledge of the detailed underlying system dynamics, the GP MPC has a 43% higher overshoot and 25% slower response time, but the GP MPC eliminates the requirement of the underlying true system model and the model simplification process involving expert knowledge.

Acknowledgements

The first author would like to acknowledge the Competence Centre Combustion Processes, KCFP, and the Swedish Energy Agency (grant number 22485-4) for the financial support. The Chinese Scholarship Council is also thanked for the sponsorship of living expenses during the first author's research. Rolf Johansson is a member of the LCCC Linnaeus Center and the eLLIIT Excellence Center at Lund University. The work described in this paper is partially supported by Shenzhen Fundamental Research (General Program)(WDZC20231129163533001).

Contribution

Xiufei Li: Investigation, Methodology, Validation, Original draft, Writing – review & editing. Miao Zhang: Investigation, Methodology, Writing – review & editing. Yuanxin Qi: Investigation, Data generating, Software. Miao Yang: Supervision, Original draft, Writing – review & editing.

References

[1] A. Baroutaji, A. Arjunan, M. Ramadan, J. Robinson, A. Alaswad, M. A. Abdelkareem, and A.-G. Olabi, "Advancements and prospects of thermal management and waste heat recovery of PEMFC," *International Journal of Thermofluids*, vol. 9, p. 100064, 2021.

[2] X. Zhang, S. Yu, M. Wang, S. Dong, J. Parbey, T. Li, and M. Andersson, "Thermal stress analysis at the interface of cathode and electrolyte in solid oxide fuel cells," *International Communications in Heat and Mass Transfer*, vol. 118, p. 104831, 2020.

[3] J. Liang, Y. Wang, Q. Liu, Y. Luo, T. Li, H. Zhao, S. Lu, F. Zhang, A. M. Asiri, F. Liu *et al.*, "Electrocatalytic hydrogen peroxide production in acidic media enabled by NiS 2 nanosheets," *Journal of Materials Chemistry A*, vol. 9, no. 10, pp. 6117–6122, 2021.

[4] M. Y. Silaa, M. Derbeli, O. Barambones, and A. Cheknane, "Design and implementation of high order sliding mode control for PEMFC power system," *Energies*, vol. 13, no. 17, p. 4317, 2020.

[5] S. Quan, Y.-X. Wang, X. Xiao, H. He, and F. Sun, "Feedback linearization-based mimo model predictive control with defined pseudo-reference for hydrogen regulation of automotive fuel cells," *Applied Energy*, vol. 293, p. 116919, 2021.

[6] S. Hahn, J. Braun, H. Kemmer, and H.-C. Reuss, "Adaptive operation strategy of a polymer electrolyte membrane fuel cell air system based on model predictive control," *International Journal of Hydrogen Energy*, vol. 46, no. 33, pp. 17 306–17 321, 2021.

[7] R. Long, S. Quan, L. Zhang, Q. Chen, C. Zeng, and L. Ma, "Current sharing in parallel fuel cell generation system based on model predictive control," *International Journal of Hydrogen Energy*, vol. 40, no. 35, pp. 11 587–11 594, 2015.

[8] M. Mehrpooya, B. Ghorbani, B. Jafari, M. Aghbashlo, and M. Pouriman, "Modeling of a single cell micro proton exchange membrane fuel cell by a new hybrid neural network method," *Thermal Science and Engineering Progress*, vol. 7, pp. 8–19, 2018. [Online]. Available: https://www.sciencedirect.com/science/article/pii/S2451904917303888

[9] I.-S. Han and C.-B. Chung, "Performance prediction and analysis of a PEM fuel cell operating on pure oxygen using data-driven models: A comparison of artificial neural network and support vector machine," *International Journal of Hydrogen Energy*, vol. 41, no. 24, pp. 10 202–10 211, 2016. [Online]. Available: https://www.sciencedirect.com/science/article/pii/S036031991530389X

[10] G. Pillonetto, F. Dinuzzo, T. Chen, G. De Nicolao, and L. Ljung, "Kernel methods in system identification, machine learning and function estimation: A survey," *Automatica*, vol. 50, no. 3, pp. 657–682, 2014. [Online]. Available: https://www.sciencedirect.com/science/article/pii/S000510981400020X

[11] Y.-J. He and Z.-F. Ma, "A data-driven Gaussian process regression model for two-chamber microbial fuel cells," *Fuel Cells*, vol. 16, no. 3, pp. 365–376, 2016. [Online]. Available: https://onlinelibrary.wiley.com/doi/abs/10.1002/fuce.201500109

[12] L. Zhu and J. Chen, "Prognostics of PEM fuel cells based on Gaussian process state space models," *Energy*, vol. 149, pp. 63–73, 2018. [Online]. Available: https://www.sciencedirect.com/science/article/pii/S0360544218302421

[13] H. Zhang, J. Jiang, H. Qin, W. Zhao, X. Li, and J. Li, "Fuel adaptive analysis and methane conversion rate prediction based on Gaussian process regression for an SR-SOFC system," in *39th Chinese Control Conference (CCC)*, Shenyang, Liaoning, China, July 2020, pp. 5407–5412.

[14] J. Li, T. Yu, and B. Yang, "Adaptive controller of PEMFC output voltage based on ambient intelligence large-scale deep reinforcement learning," *IEEE Access*, vol. 9, pp. 6063–6075, 2021.

[15] X. Li, Y. Qi, S. Li, P. Tunestål, and M. Andersson, "A multi-input and single-output voltage control for a polymer electrolyte fuel cell system using model predictive control method," *International Journal of Energy Research*, vol. 45, no. 9, pp. 12 854–12 863, 2021. [Online]. Available: https://onlinelibrary.wiley.com/doi/abs/10.1002/er.6616

[16] C. Rasmussen and C. Williams, *Gaussian Processes for Machine Learning*. Cambridge, MA, USA: MIT Press, Jan. 2006.

[17] D. C. Liu and J. Nocedal, "On the limited memory BFGS method for large scale optimization," *Mathematical programming*, vol. 45, no. 1, pp. 503–528, 1989.

[18] A. G. Baydin, B. A. Pearlmutter, A. A. Radul, and J. M. Siskind, "Automatic differentiation in machine learning: A survey," *Journal of Machine Learning Research*, vol. 18, no. 153, pp. 1–43, 2018. [Online]. Available: http://jmlr.org/papers/v18/17-468.html

[19] C. Ziogou, S. Voutetakis, M. C. Georgiadis, and S. Papadopoulou, "Model predictive control (MPC) strategies for PEM fuel cell systems – A comparative experimental demonstration," *Chemical Engineering Research and Design*, vol. 131, pp. 656–670, 2018, energy Systems Engineering. [Online]. Available: https://www.sciencedirect.com/science/article/pii/S0263876218300261